ACS OMEGA

http://pubs.acs.org/journal/acsodf

Article

InP and AlInP(001)(2 × 4) Surface Oxidation from Density Functional Theory

Isaac Azahel Ruiz Alvarado,* Marsel Karmo, Erich Runge, and Wolf Gero Schmidt

Cite This: *ACS Omega* 2021, 6, 6297−6304

Read Online

ACCESS | Metrics & More | Article Recommendations | Supporting Information

ABSTRACT: The atomic structure and electronic properties of the InP and $Al_{0.5}In_{0.5}P(001)$ surfaces at the initial stages of oxidation are investigated via density functional theory. Thereby, we focus on the mixed-dimer (2 × 4) surfaces stable for cation-rich preparation conditions. For InP, the top In−P dimer is the most favored adsorption site, while it is the second-layer Al−Al dimer for AlInP. The energetically favored adsorption sites yield group III−O bond-related states in the energy region of the bulk band gap, which may act as recombination centers. Consistently, the In p state density around the conduction edge is found to be reduced upon oxidation.

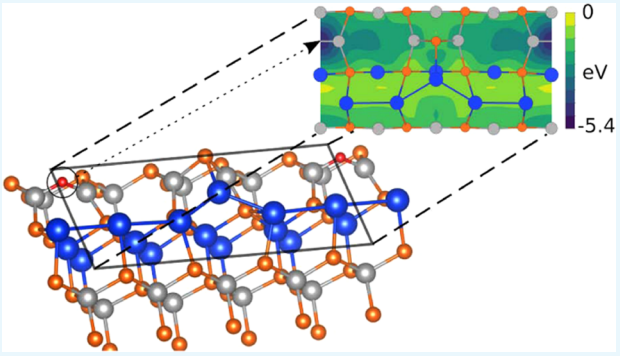

INTRODUCTION

III−V compound semiconductors, such as indium phosphide, and their ternary and quaternary alloys, find extensive applications in high-speed integrated circuits,[1,2] photonic devices,[3] and high-efficiency solar cells or artificial leaves for solar-to-hydrogen conversion,[4] and they continue to be of great interest in contemporary fields of study, e.g., nano-technological applications such as nanowires[5] and quantum dots.[6] Most of these devices are based on, often alloy-based, heterojunctions or quantum wells. The oxides that form on these devices can strongly affect their performance.[7] Therefore, it is important to explore the oxide/compound semiconductor interface. The surface structures and electronic properties of the III−V phosphide compounds have been determined about two decades ago; see, e.g., refs 8−12. Comparatively little is known, however, about III−V alloy surfaces and the microscopic details of III−V surfaces exposed to oxygen or water.[13−15] Chen and co-workers[16] concluded from their X-ray photoelectron spectroscopy (XPS), reflectance anisotropy spectroscopy (RAS), and low-energy electron diffraction (LEED) data that InP(001) oxidation is an activated process and strongly surface structure-dependent. Depending on the specific surface structure, O_2 adsorbs dissociatively and gets inserted into In−In and In−P bonds. The formation of P−O−In and In−O−In bonds has been confirmed by density functional theory (DFT) calculations.[17] May et al.[18] explored the initial interaction of water and oxygen with atomically well-defined surfaces of InP(100) using RAS. They concluded from their data that water adsorption mainly leads to the formation of In−O−P bonds, while exposure to molecular oxygen, in contrast, shows a higher tendency to form In−O−In bonds as well as a tendency for O to diffuse toward the bulk. The surface oxidation details depend not only on the specific surface structure, e.g., the oxidation of cation-rich or anion-rich surfaces, but also on the respective cations and anions. May and Sprik noted, for example, that the P-rich GaP(100) surface undergoes a surface reordering upon contact with gas-phase water, but does not oxidize.[19] For Ga-rich GaP(001) surface, Jeon and co-workers[20] found a Ga−O−Ga bond formation after adsorption of a water molecule and subsequent decomposition. The oxidation of $Al_xIn_{1-x}P$, on the other hand, was found to occur faster with a higher Al content[21] and to result in oxide layers with excellent insulating properties.[22]

The present paper aims at improving our understanding of III−V(001) surface oxidation by comparing density functional theory (DFT) data for the prominent mixed-dimer InP(001)(2 × 4) surface with results for $Al_{0.5}In_{0.5}P(001)(2 \times 4)$ structures favorable for cation-rich preparation conditions. Thereby, we focus on CuPt-type ordered crystals, i.e., with alternating group III layers perpendicular to the $[\bar{1}11]$ or $[1\bar{1}1]$ direction, as formed spontaneously in metalorganic vapor-phase epitaxy-grown AlInP epilayers.[23]

RESULTS AND DISCUSSION

The stability of InP(001) has been investigated previously.[10] The mixed-dimer (2 × 4) surface (cf. Figure 2) is stable for a

Received: December 10, 2020
Accepted: February 11, 2021
Published: February 25, 2021

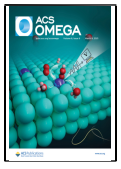

https://dx.doi.org/10.1021/acsomega.0c06019
ACS Omega 2021, 6, 6297−6304

wide range of In-rich preparation conditions and will be exclusively studied here.

The equilibrium atomic structures of AlInP(001) surfaces are essentially unknown. Therefore, we perform total-energy calculations for various CuPt-B-type $Al_{0.5}In_{0.5}P(001)$ surface structures derived from the plethora of stable III−V(001) surfaces.[9,10] Four of these structures are found to be stable, as can be seen in the phase diagram in Figure 1 and 2.

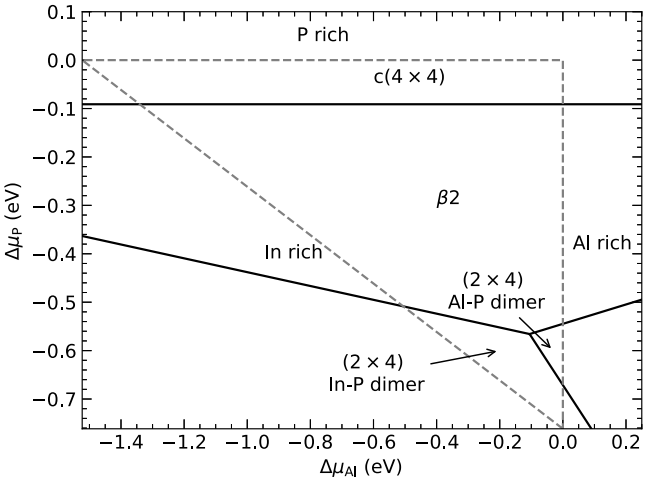

Figure 1. Dependence of energetically favored AlInP(001) surface structures, see Figure 2, on the Al and P chemical potentials. The thermodynamically allowed range of the chemical potentials according to eqs 2 and 5 is indicated by the dashed lines.

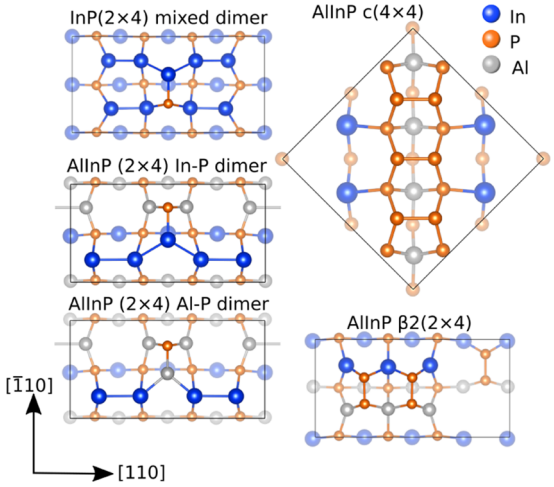

Figure 2. Top view of stable relaxed InP and AlInP(001) surface structures. The color scheme and notation for the crystallographic directions used here are also applied in the subsequent figures.

Interestingly, the In−P and Al−P mixed-dimer (2 × 4) surface structures stable for cation-rich preparation conditions differ from the InP mixed-dimer (2 × 4) surface in terms of the second-layer cation arrangement: The difference in the In and Al covalent radii leads to a staggered arrangement of the second-layer cation dimers in the case of the ternary compound; cf. Figures 2 and 3.

Next, we explore the oxidation of the cation-rich mixed-dimer (2 × 4) surfaces. First, we calculate the potential energy surface (PES) for a single adsorbed oxygen atom. A lateral mesh of 5 × 10 equidistant points is used to map the

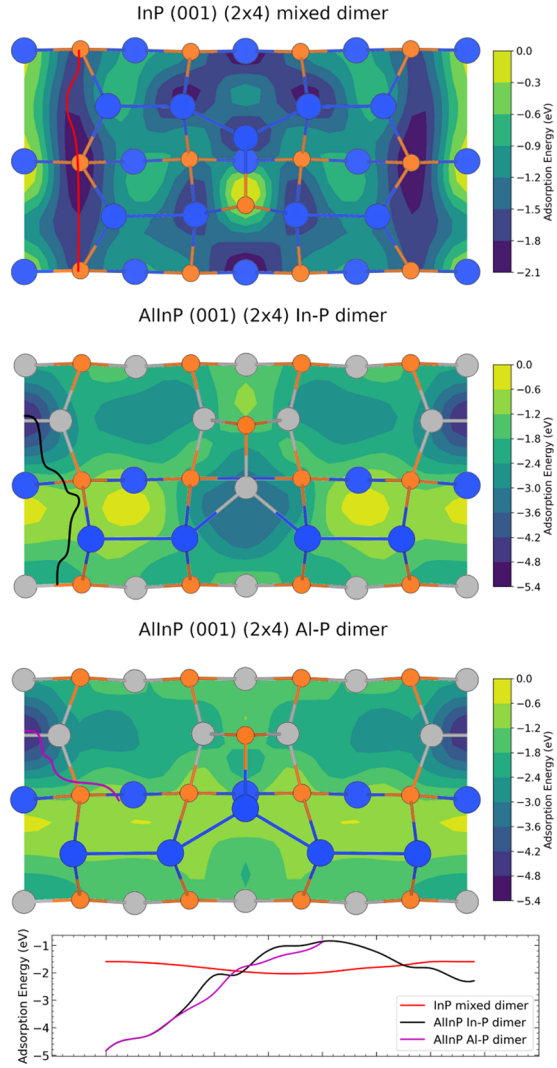

Figure 3. Calculated potential energy surfaces (PES) for single oxygen adsorption on the cation-rich InP and AlInP(001)(2 × 4) surfaces. The lowest-energy paths for diffusion are indicated in the PES and compared energetically in the bottom panel.

adsorption energy. In the calculations, the oxygen adatom is positioned on these points, and allowed only to relax along the surface normal. The substrate structural degrees of freedom are freely relaxed. The adsorption energies thus calculated refer to the spin-triplet ground state of molecular oxygen. The PES obtained in this way gives indications for the most favorable adsorption sites. The results are shown in Figure 3. As obvious from the calculated data, there are qualitative differences between the O adsorption characteristics on InP and AlInP: (i) For the ternary surface, the maximum adsorption energy is more than twice the value obtained for the binary compound. In particular, adsorption on Al−Al bonds is energetically favorable. This is in accordance with the higher heat of formation of aluminum oxide (−17.37 eV[24]) compared to indium oxide (−9.57 eV[25]). (ii) Furthermore, the calculated PES suggest a different O diffusion behavior (see Figure 3, bottom). Oxygen atoms on the InP(001)(2 × 4) surface can be expected to diffuse along the [1̄10] direction, parallel to the InP dimer, hindered by rather shallow barriers of ∼0.3 eV. On the ternary surfaces, in contrast, diffusion is hindered by considerably larger barriers of ∼2 to 4 eV. This is related to the

https://dx.doi.org/10.1021/acsomega.0c06019
ACS Omega 2021, 6, 6297−6304

very favorable O adsorption on surface Al cations. (iii) The III−V bond of the topmost dimer is a favorable O adsorption site for InP, in contrast to AlInP, where it is outfavored by adsorption close to second-layer Al−Al dimer.

Starting from the most favorable O adsorption sites, derived from the PES, we explore adsorption on InP and AlInP(001) surfaces, as well as insertion into deeper layers. To do so, we explored the following bonding sites: top In−P dimer, In−P bonds between the first and second layers, second-layer In−In dimers, and In−P bonds formed by the second and third layers. In the case of the ternary surfaces, the following sites were probed: second-layer Al−Al dimers, trench between the Al−Al dimers, top cation-P dimer, and Al−In bonds between the first and second layers. In the case of substitutive insertion, all atoms within the uppermost three layers were tentatively replaced by oxygen. Altogether, considering all possible combinations, more than 600 starting geometries were structurally relaxed and analyzed with respect to their energetics. The complete set of energetically relevant structures considered here for O adsorption and substitution on the mixed-dimer InP(001)(2 × 4) surface can be seen in Figures S1 and S2 in the Supporting Information (SI). Figure 4 summarizes the most favorable geometries.

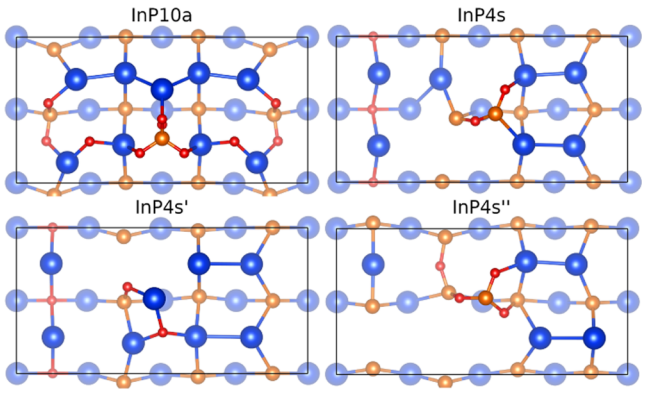

Figure 4. Energetically favorable O adsorption and substitution structures calculated for the mixed-dimer InP(001)(2 × 4) surface. The number in the notation indicates the number of O atoms adsorbed (a) or substituted (s). The complete set of relevant structures considered in the present work is shown in Figures S1 and S2 in the Supporting Information.

To compare these structures energetically, the complete thermodynamically allowed range of the In chemical potential, $-0.41 \leq \Delta\mu_{In} \leq 0$, was probed. It turns out, however, that the specific choice does not affect the general trend. Therefore, we assume in the following discussion an intermediate value of the In chemical potential, $\Delta\mu_{In} = -0.2$ eV, and vary the oxygen chemical potential. As can be seen in Figure 5, the surface thermodynamic stability increases with increasing oxygen content, even for a low oxygen partial pressure. This clearly indicates, even without explicit calculation of barriers, that as long as oxygen is available, the oxidation process is only kinetically hindered. Similar results were obtained earlier for the oxidation of Si(001) surfaces.[26] Our results agree with the experimental findings for the InP(001)(2 × 4) surface: Chen et al.[27] report that the In-rich InP(001) surface is highly reactive toward oxygen and rapidly forms an oxide layer even at a low oxygen exposure at 300 K. A more detailed view of the energetics of oxygen-substituted surfaces is shown in Figure 6.

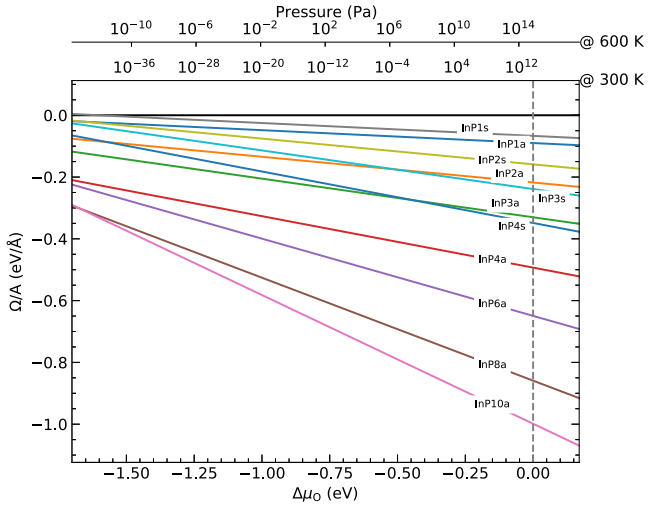

Figure 5. Surface grand-canonical potential vs oxygen chemical potential of the energetically most favored O adsorption and substitution geometries for InP. For the P chemical potential, an intermediate value, $\Delta\mu_{In} = -0.2$ eV, is assumed. The O chemical potential on the bottom axis is given relative to molecular oxygen. The temperature and pressures are given by eq 6.

Obviously, only very low values of the O chemical potential will cease the oxidation.

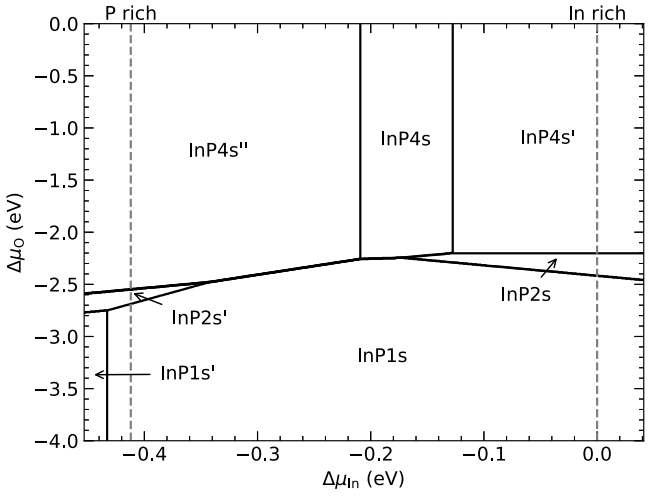

Figure 6. Phase diagram of the most energetically favored O substitution geometries of InP(001) in the stability range of the In chemical potential given by eqs 2 and 3 (dashed lines) and in dependence on the O chemical potential.

In particular, substitutional oxidation can be expected to lead to a rapid loss of surface order (see Figure 4). Most commonly, In−O−P bonds are formed during oxidation. This occurs in all stable O adsorption geometries. In−O−In bonds appear slightly less favored. This corresponds well to the experimental findings of May et al.[18] Oxygen substitution reactions under oxygen-rich conditions ($\Delta\mu_O = 0$) replace In and P atoms with roughly equal probability. The tendency to substitute surface In or P atoms for low values of the O chemical potential ($\Delta\mu_O \ll 0$) depends on the phosphorous chemical potential (see Figure 6). The P replacement results in oxygen atoms that are two-, three-, and fourfold coordinated to In atoms (see Figure S2 in the SI), as previously found in refs 17, 28. P−O−P bonds

https://dx.doi.org/10.1021/acsomega.0c06019
ACS Omega 2021, 6, 6297−6304

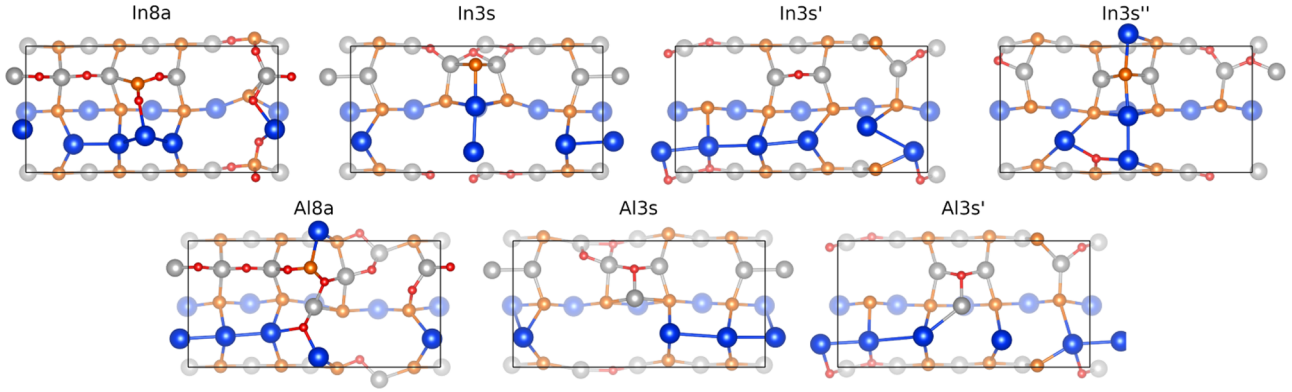

Figure 7. Energetically favorable O adsorption and substitution structures calculated for AlInP(001)(2 × 4) surfaces derived from the InP (top row) and AlP mixed-dimer models (bottom row), respectively. The complete set of relevant structures considered in the present work is shown in Figures S1−S6 in the SI.

are less frequent. The threefold O coordinated on the top dimer is the most stable substitution, as observed during initial substitution (see Figure S1, InP1s). In the case of oxidized GaAs(001) surfaces, O bonding to anion−anion dimers was observed by Yi et al.,[14] while the preferential formation of Ga−O−Ga bonds was observed in ref 15. In the case of the GaP(001)(2 × 4) mixed-dimer surface, water adsorption was found to lead to Ga−O−Ga bonds, and, energetically less favored, Ga−O−P bonds.[20]

The energetically stable oxygen-adsorbed and oxygen-substituted AlInP(001)(2 × 4) surface structures explored here are shown in Figures S3−S6 in the SI. Figure 7 summarizes the most relevant geometries. Energetically, we observe similarities to the binary case. The stability of the surface increases with the amount of oxygen; see Figure 8. The adsorption of eight O atoms, i.e., the highest number investigated here, leads to the most stable geometries for a very large range of the oxygen chemical potential for both the Al−P and In−P mixed-dimer derived structures. As in the binary case, this indicates that as long as oxygen is available, the oxidation process is only kinetically hindered. In the case of substitutional O, the P atom replacements are the most common, as can be seen in Figure 9. Besides these similarities, there are also differences to the binary case: In contrast to the In−O−P and In−O−In bonds, which are most common for binary surfaces, Al-containing bonds Al−O−P, Al−O−Al, and In−O−Al are most frequently formed at O-adsorbed ternary surfaces. The second-layer Al−Al dimer is the preferred adsorption site, leading to Al−O−Al bonds. In addition, we find O coordinated to two In and one P as well as coordinated to two Al and one P. Substitutional oxidation of ternary surfaces leads most frequently to Al−O−Al bonds, compared to the In−O−In-type bonds found in the binary case. Oxygen adsorption on Al−P and In−P mixed-dimer AlInP surfaces follows a similar pattern and results in similar geometries that differ, however, from the adsorption on InP. This behavior is due to second-layer Al−Al dimers being the most favorable adsorption site for oxygen on ternary surfaces; see Figure 3. A trench along the $[\bar{1}10]$ direction forms as a result of the bonds breaking and bond rearrangement in the second layer. As already observed for InP, substitutional oxidation can be expected to lead to a rapid loss of surface order; see Figure 7.

To explore the influence of the oxidation on the III−V surface electronic properties, we calculate the density of states (DOS) for the most relevant geometries. The clean InP surface

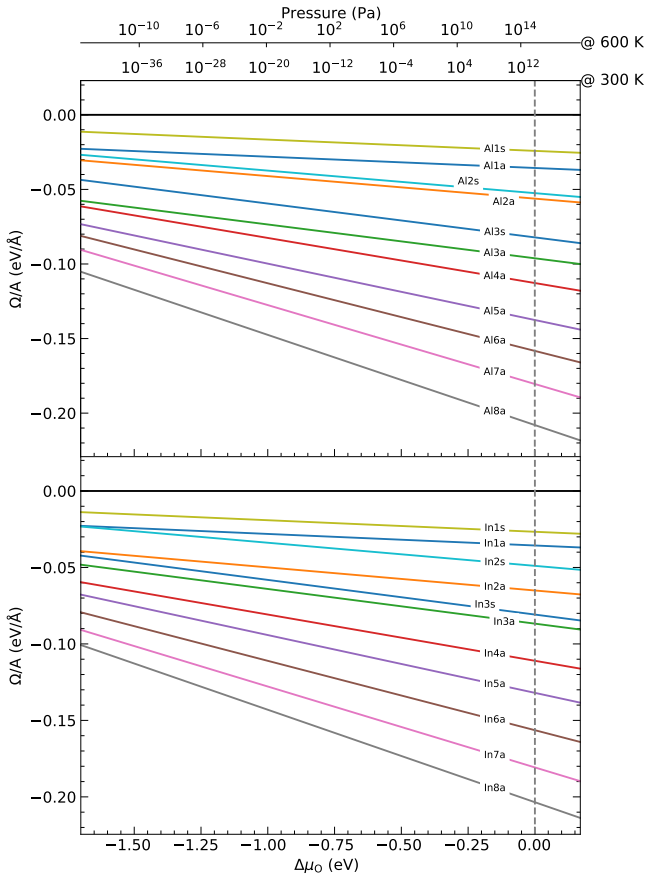

Figure 8. Surface grand-canonical potential vs oxygen chemical potential of the energetically most favored O adsorption and substitution geometries of AlInO(001). The O chemical potential on the bottom axis is given relative to molecular oxygen. The data calculated for the Al−P and In−P mixed-dimer structures are shown in the top and bottom panels, respectively.

is characterized by a high density of In and P p states at the valence band edge, while the conduction band edge is dominated by In p and s states; see Figure 10a. Adsorption of oxygen induces in some instances a midgap state, composed primarily of In, P, and O p states; see Figures 10b and S7 in the SI. The appearance of this state is closely correlated to the oxygen coordination of surface P atoms and corresponds to an O-modified P dangling bond. Oxygen adsorption also reduces

https://dx.doi.org/10.1021/acsomega.0c06019
ACS Omega 2021, 6, 6297−6304

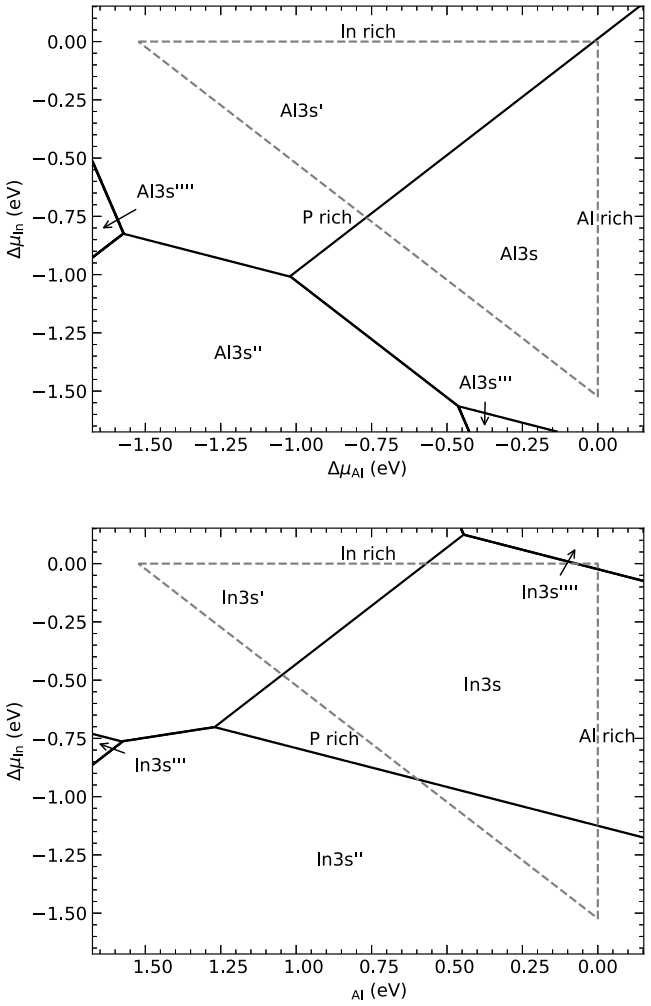

Figure 9. Phase diagram of the most energetically favored O substitution geometries of AlInP(001) in the stability range of the In and Al chemical potential given by eqs 2 and 3; assuming O-rich preparation conditions, $\Delta\mu_O = 0$ eV. The data calculated for the Al−P and In−P mixed-dimer structures are shown in top and bottom, respectively.

the DOS at about 0.8 eV above the conduction band minimum (CBM). This is due to a reduced contribution of In p states, more precisely the dangling bonds of second-layer In atoms; cf. refs 17, 29. The sensitivity of this state to InP surface oxidation has been noted earlier by time-resolved two-photon photoemission spectroscopy.[30] Experimentally, the state was detected about 0.85 eV above the conduction band edge, close to the present findings.

The influence of oxygen adsorption on the electronic properties of the AlInP surfaces derived from the Al−P and In−P mixed-dimer models is shown in Figures 10c,d and S8 as well as in Figures 10e,f and S9, respectively. Overall, we find that Al-derived states contribute only little to the valence and conduction band edges. A particular Al-related DOS feature of the In−P surface, derived from Al p states, is located at ca. −0.25 eV in energy. In the Al−P surface, this feature is closer to the valence band maximum (VBM) at ca. −0.1 eV, which can be related to the higher Al content in the surface. Through the initial stages of oxidation, the DOS maintains a similar profile, suggesting that subsequent midgap states (at increased oxidation) are independent of the Al−O bonds. The valence bands are mostly composed of P and In p states, as in the binary surface. However, there is a slightly stronger P contribution near the band gap. Indium p states dominate near the CBM. In the case of the Al−P mixed-dimer model, In-derived states appear above the bulk VBM. This feature disappears upon oxidation. At the same time, the In p state contribution near the conduction band edge is reduced, and an In s state emerges below the CBM; see Figures 10d and S8. These changes are related to the rearrangement of the second-layer In atoms upon trench formation; see Figure 7. Phosphorous-related p states emerge below the CBM, as more oxygen is adsorbed to the third-layer P and O−P bonds form.

The In−P mixed-dimer model differs from the Al−P case, as it does not form an additional state above the bulk VBM. Rather, it is characterized by an additional In p state below the bulk CBM; see Figure 10e. Upon oxidation, this state is pushed up in energy; see Figures 10f and S9. Similar to the case of the Al−P model, this is related to the formation of a trench by a rearrangement of the second-layer In atoms. As oxidation increases, and an In−O−P bond is formed in the top dimer, the In p contribution on the CBM is reduced (cf. s9 In4a). Therefore, the top In−P surface is responsible for the In p midgap state. Furthermore, for higher O coverages, the P p states in the valence band are pushed up upon In−O−P bond formation between the second- and third-layer atoms.

Altogether, it is clear from the calculations here that the initial stages of oxygen adsorption do not lead to passivation of III−V(001) surface states. Rather, the existing states are modified, and new states appear, in many instances in the region of the bulk band gap. These states may behave as charge traps that affect the carrier generation and recombination process at the interface and thus worsen the electric and optical efficiency. Thus, strategies to avoid the formation of Al/In oxides at the surface are needed. May et al.[4] used Rh deposition to transform AlInP surfaces, leading to the formation of a PO_x layer and thereby achievement of the passivation of the surface, increasing the efficiency.

CONCLUSIONS

In conclusion, the present DFT calculations show that the AlInP(001) surface geometries are different from that of InP: While cation−anion heterodimers form in the topmost layer for both surfaces in cation-rich preparation conditions, the second-layer dimer arrangement is different. Even larger differences are observed concerning the oxidation. The Al−Al dimers provide more favorable O adsorption sites than found on InP surfaces. This is related to the considerably larger heat of formation of aluminum oxide compared to indium oxide and explains experimental findings that suggest the oxidation of $Al_xIn_{1-x}P$ to occur faster with higher Al content. Oxidation of AlInP leads more frequently to Al−O bonds than to In−O bonds. The oxygen diffusion characteristics of InP and AlInP(001) differ. Oxygen diffusion on InP is hindered only by relatively small barriers of about 0.3 eV and may occur along the $[\bar{1}10]$ direction. In contrast, O diffusion is practically excluded on AlInP. Concerning substitutional adsorption, P atoms are more likely to be replaced by O than Al or In. This matches with the energetic preference of Al/In oxidation. As oxidation increases, we observe the emergence of states in the bulk band gap region. These states arise from III−O bonds and are expected to reduce the electronic efficiency of the oxide layer by providing charge traps. In combination with the high surface reactivity toward oxygen, detrimental effects on the

https://dx.doi.org/10.1021/acsomega.0c06019
ACS Omega 2021, 6, 6297−6304

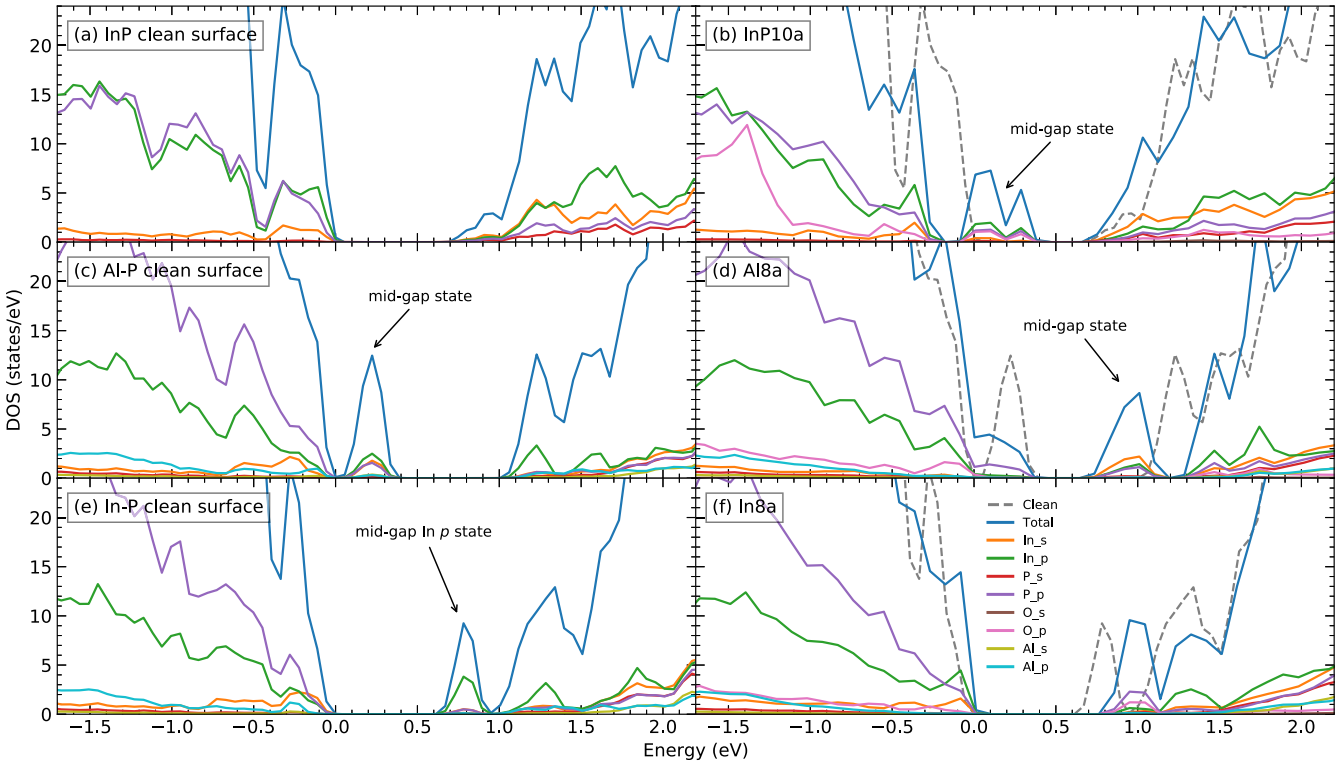

Figure 10. Electron density of states calculated for the mixed-dimer InP(001)(2 × 4) surface (a), the InP10a model (b), the Al−P mixed-dimer AlInP(001)(2 × 4) surface (c), the Al8a model (d), the In−P mixed-dimer AlInP(001)(2 × 4) surface (e), and the In8a model (f). In addition to the total DOS, species-resolved s and p contributions are shown.

electronic and optical surface and interface properties may result.

METHODOLOGY

In detail, the DFT calculations are performed using the Vienna Ab initio Simulation Package (VASP).[31] The generalized gradient approximation (GGA) with the Perdew−Burke−Ernzerhof (PBE)[32] functional is used to model the electron exchange−correlation interaction. The electron−ion interaction is described by the projector-augmented wave (PAW) scheme.[33,34] The electronic wave functions are expanded into plane waves up to a kinetic energy cutoff of 500 eV. The Brillouin zone integration is performed using Γ-centered 3 × 6 × 1 meshes. The (001) surfaces are modeled by supercells containing 8 and 13 atomic layers (each containing 8 atoms in the ideal case) for InP and AlInP, respectively, and a vacuum region of ∼12 Å. The AlInP supercells were modeled according to the CuPt-B-type crystal ordering. The slab bottom dangling bonds are saturated with fractionally charged H atoms (Z = 1.25 and 0.75 for group III and V atoms, respectively). The electric field resulting from the inequivalence of the two surfaces is taken into account by a dipole correction to the electrostatic potential. The atoms are considered to be in their relaxed ground-state positions when the forces acting on the ions are lower than 0.02 eV/Å. The InP and AlInP calculations are performed at the respective equilibrium lattice parameters of 6.001 and 5.745 Å, which are close to the corresponding low-temperature experimental values of 5.87 and 5.67 Å.

To compare the various clean and oxidized surfaces energetically, one must take into account the chemical potentials μ_{A_i} of the respective surface constituents. The surface ground state is determined by the thermodynamic potential minimum

$$\Omega = U - \mathrm{TS} - \sum_i \mu_{A_i} n_{A_i} \tag{1}$$

where U is the total energy of the system. In solids, the entropy term, TS, contributes very little to the difference in Ω under usual experimental conditions and is neglected in the following.[35] The chemical potentials μ_{A_i} for A_i = In, Al, and P are restricted by their bulk values

$$\mu_{A_i} \leq \mu_{A_i,\mathrm{bulk}} \tag{2}$$

Furthermore, in the case of InP surfaces, they are related to each other by

$$\mu_{\mathrm{In}} + \mu_{\mathrm{P}} = \mu_{\mathrm{InP,bulk}} = \mu_{\mathrm{In,bulk}} + \mu_{\mathrm{P,bulk}} - \Delta H_{\mathrm{f,InP}} \tag{3}$$

with $\Delta H_{\mathrm{f,InP}}$ being the heat of formation of InP. Consequently, the formation energy may be written as a function of a single variable, which we will take to be $\Delta\mu_{\mathrm{In}}$

$$-\Delta H_{\mathrm{f,InP}} \leq \Delta\mu_{\mathrm{In}} := \mu_{\mathrm{In}} - \mu_{\mathrm{In,bulk}} \leq 0 \tag{4}$$

This limit can be related to preparation conditions: $\Delta\mu_{\mathrm{In}} = 0$ corresponds to In-rich conditions, where the surface In atoms are in equilibrium with bulk In. $\Delta\mu_{\mathrm{In}} = -\Delta H_{\mathrm{f,InP}}$ corresponds to In-poor conditions, where the surface P atoms are in equilibrium with bulk P.

A single chemical potential is not sufficient to characterize the stability of $Al_{0.5}In_{0.5}P(001)$ surfaces. In this case, the relation

https://dx.doi.org/10.1021/acsomega.0c06019
ACS Omega 2021, 6, 6297−6304

$$\mu_{Al} + \mu_{In} + 2\mu_P = 2\mu_{Al_{0.5}In_{0.5}P,bulk} = \mu_{Al,bulk} + \mu_{In,bulk} + 2\mu_{P,bulk} - 2\Delta H_{f,Al_{0.5}In_{0.5}P} \quad (5)$$

allows us to formulate the formation energy depending on $\Delta\mu_P$ and $\Delta\mu_{Al}$. For the heats of formation $\Delta H_{f,InP}$ and $\Delta H_{f,AlInP}$, we calculate values of −0.41 and −1.52 eV, respectively.

In the case of oxidized surfaces, the oxygen chemical potential provides an additional and independent degree of freedom. In the approximation of a two-atomic ideal gas, it is written depending on partial pressure p and temperature T as

$$\Delta\mu_O(p, T) = \frac{k_B T}{2}\left[\ln\left\{\frac{p\lambda^3}{k_B T}\right\} - \ln Z_{rot} - \ln Z_{vib}\right] - \frac{1}{2}U_{O_2} \quad (6)$$

where k_B is the Boltzmann constant, λ is the de Broglie thermal wavelength of the O_2 molecule

$$\lambda = \sqrt{\frac{2\pi\hbar^2}{mk_B T}} \quad (7)$$

and Z_{rot} and Z_{vib} are its rotational and vibrational partition functions, respectively.

■ ASSOCIATED CONTENT

Supporting Information

The Supporting Information is available free of charge at https://pubs.acs.org/doi/10.1021/acsomega.0c06019.

Relevant InP(001) and AlInP(001)(2 × 4) surface geometries and calculated density of states for relevant surface structures (PDF)

■ AUTHOR INFORMATION

Corresponding Author

Isaac Azahel Ruiz Alvarado − *Lehrstuhl für Theoretische Materialphysik, Universität Paderborn, 33095 Paderborn, Germany;* orcid.org/0000-0002-4710-1170; Email: azahel@mail.upb.de

Authors

Marsel Karmo − *Institut für Physik, Technische Universität Ilmenau, 98693 Ilmenau, Germany*

Erich Runge − *Institut für Physik, Technische Universität Ilmenau, 98693 Ilmenau, Germany*

Wolf Gero Schmidt − *Lehrstuhl für Theoretische Materialphysik, Universität Paderborn, 33095 Paderborn, Germany;* orcid.org/0000-0002-2717-5076

Complete contact information is available at: https://pubs.acs.org/10.1021/acsomega.0c06019

Notes

The authors declare no competing financial interest.

■ ACKNOWLEDGMENTS

Financial support by DFG (SCHM1361/26, RU1383/6) is gratefully acknowledged. The authors thank the Paderborn Center for Parallel Computing (PC^2) and the Höchstleistungs-Rechenzentrum Stuttgart (HLRS) for grants of high-performance computer time.

■ REFERENCES

(1) Kobayashi, K. W.; Cowles, J.; Tran, L. T.; Gutierrez-Aitken, A.; Block, T. R.; Oki, A. K.; Streit, D. C. A 50-MHz-55-GHz multidecade InP-based HBT distributed amplifier. *IEEE Microwave Guided Wave Lett.* **1997**, *7*, 353−355.

(2) Mullrich, J.; Thurner, H.; Mullner, E.; Jensen, J. F.; Stanchina, W. E.; Kardos, M.; Rein, H. M. High-gain transimpedance amplifier in InP-based HBT technology for the receiver in 40-Gb/s optical-fiber TDM links. *IEEE J. Solid-State Circuits* **2000**, *35*, 1260−1265.

(3) Yap, D.; Elliott, K. R.; Brown, Y. K.; Kost, A. R.; Ponti, E. S. High-speed integrated optoelectronic modulation circuit. *IEEE Photonics Technol. Lett.* **2001**, *13*, 626−628.

(4) May, M. M.; Lewerenz, H.-J.; Lackner, D.; Dimroth, F.; Hannappel, T. Efficient direct solar-to-hydrogen conversion by in situ interface transformation of a tandem structure. *Nat. Commun.* **2015**, *6*, No. 8286.

(5) Ugarte, D.; Tizei, L.; Cotta, M.; Ducati, C.; Midgley, P.; Eggeman, A. Analysis of structural distortion in Eshelby twisted InP nanowires by scanning precession electron diffraction. *Nano Res.* **2019**, *12*, 939−946.

(6) Wu, S.; Peng, K.; Battiato, S.; Zannier, V.; Bertoni, A.; Goldoni, G.; Xie, X.; Yang, J.; et al. Anisotropies of the g-factor tensor and diamagnetic coefficient in crystal-phase quantum dots in InP nanowires. *Nano Res.* **2019**, *12*, 2842−2848.

(7) Driad, R.; McKinnon, W. R.; Lu, Z. H.; McAlister, S. P. Effect of UV-ozone oxidation on the device characteristics of InP-based heterostructure bipolar transistors. *J. Electron. Mater.* **2000**, *29*, L33−L36.

(8) Tsai, M.-H.; Liu, C. F.; Hsu, L.-K. P-terminated InP(100) surface studied using a first-principles energy-minimization approach. *Phys. Rev. B* **1998**, *58*, 6764−6767.

(9) Schmidt, W. G. (4 × 2) and (2 × 4) reconstructions of GaAs and InP(001) surfaces. *Appl. Phys. A: Mater. Sci. Process.* **1997**, *65*, 581−586.

(10) Schmidt, W. G. III-V Compound Semiconductor (001) Surfaces. *Appl. Phys. A: Mater. Sci. Process.* **2002**, *75*, 89−99.

(11) Schmidt, W. G.; Hahn, P. H.; Bechstedt, F.; Esser, N.; Vogt, P.; Wange, A.; Richter, W. InP(001)(2 × 1) surface: A hydrogen-stabilized structure. *Phys. Rev. Lett.* **2003**, *90*, No. 126101.

(12) Li, D. F.; Liu, K. Z.; Xiao, H. Y.; Dong, H. N.; Zu, X. T. First-principles study of GaP(001) surfaces. *J. Alloys Compd.* **2007**, *440*, 229−235.

(13) Pham, T. A.; Zhang, X.; Wood, B. C.; Prendergast, D.; Ptasinska, S.; Ogitsu, T. Integrating Ab Initio Simulations and X-ray Photoelectron Spectroscopy: Toward A Realistic Description of Oxidized Solid/Liquid Interfaces. *J. Phys. Chem. Lett.* **2018**, *9*, 194−203.

(14) Yi, S. I.; Kruse, P.; Hale, M.; Kummel, A. C. Adsorption of atomic oxygen on GaAs(001)-(2 × 4) and the resulting surface structures. *J. Chem. Phys.* **2001**, *114*, 3215−3223.

(15) Placidi, E.; Hogan, C.; Arciprete, F.; Fanfoni, M.; Patella, F.; Del Sole, R.; Balzarotti, A. Adsorption of molecular oxygen on GaAs(001) studied using high-resolution electron energy-loss spectroscopy. *Phys. Rev. B* **2006**, *73*, No. 205345.

(16) Chen, G.; Visbeck, S. B.; Law, D. C.; Hicks, R. F. Structure-sensitive oxidation of the indium phosphide (001) surface. *J. Appl. Phys.* **2002**, *91*, 9362−9367.

(17) Santosh, K. C.; Wang, W.; Dong, H.; Xiong, K.; Longo, R. C.; Wallace, R. M.; Cho, K. First principles study on InP (001)-(2 × 4) surface oxidation. *J. Appl. Phys.* **2013**, *113*, No. 103705.

(18) May, M. M.; Lewerenz, H.-J.; Hannappel, T. Optical in Situ Study of InP(100) Surface Chemistry: Dissociative Adsorption of Water and Oxygen. *J. Phys. Chem. C* **2014**, *118*, 19032−19041.

(19) May, M. M.; Sprik, M. Water adsorption on the P-rich GaP(100) surface: optical spectroscopy from first principles. *New J. Phys.* **2018**, *20*, No. 033031.

(20) Jeon, S.; Kim, H.; Goddard, W. A.; Atwater, H. A. DFT Study of Water Adsorption and Decomposition on a Ga-Rich GaP(001)(2 × 4) Surface. *J. Phys. Chem. C* **2012**, *116*, 17604−17612.
(21) Graham, M. J.; Moisa, S.; Sproule, G. I.; Wu, X.; Fraser, J. W.; Barrios, P. J.; Landheer, D.; Springthorpe, A. J.; Extavour, M. Thermal oxidation of InAlP. *Mater. High Temp.* **2003**, *20*, 277−280.
(22) Cao, Y.; Zhang, J.; Li, X.; Kosel, T. H.; Fay, P.; Hall, D. C.; Zhang, X. B.; Dupuis, R. D.; Jasinski, J. B.; Liliental-Weber, Z. Electrical properties of InAlP native oxides for metal−oxide−semiconductor device applications. *Appl. Phys. Lett.* **2005**, *86*, No. 062105.
(23) Jinghua, Z.; Xiaohong, T.; Jinghua, T. Atomic ordering of AlInP grown by MOVPE at different temperatures in pure ambient N2. *CrystEngComm* **2009**, *11*, No. 1068.
(24) Cox, J.; Wagman, D.; Medvedev, V. *CODATA Key Values for Thermodynamics*; CODATA Series on Thermodynamic Properties; Hemisphere Publishing Corporation, New York, 1989.
(25) Cordfunke, E. H. P.; Konings, R. J. M.; Ouweltjes, W. The standard enthalpy of formation of In2O3. *J. Chem. Thermodyn.* **1991**, *23*, 451−454.
(26) Fuchs, F.; Schmidt, W. G.; Bechstedt, F. Initial Stage of Si(001) Surface Oxidation from First-Principles Calculations. *J. Phys. Chem. B* **2005**, *109*, 17649−17653.
(27) Chen, G.; Visbeck, S. B.; Law, D. C.; Hicks, R. F. Structure-sensitive oxidation of the indium phosphide (001) surface. *J. Appl. Phys.* **2002**, *91*, 9362−9367.
(28) Wood, B. C.; Ogitsu, T.; Schwegler, E. Local structural models of complex oxygen- and hydroxyl-rich GaP/InP(001) surfaces. *J. Chem. Phys.* **2012**, *136*, No. 064705.
(29) Schmidt, W. G.; Bechstedt, F. Geometry and electronic structure of InP(001)(2×4) reconstructions. *Surf. Sci.* **1998**, *409*, 474−484.
(30) Friedrich, D.; Sippel, P.; Supplie, O.; Hannappel, T.; Eichberger, R. Two-Photon Photoemission Spectroscopy for Studying Energetics and Electron Dynamics at Semiconductor Interfaces. *Phys. Status Solidi A* **2018**, *216*, No. e1800738.
(31) Kresse, G.; Furthmüller, J. Efficiency of ab-initio total energy calculations for metals and semiconductors using a plane-wave basis set. *Comput. Mater. Sci.* **1996**, *6*, 15−50.
(32) Perdew, J. P.; Burke, K.; Ernzerhof, M. Generalized Gradient Approximation Made Simple. *Phys. Rev. Lett.* **1996**, *77*, 3865−3868.
(33) Blöchl, P. E. Projector augmented-wave method. *Phys. Rev. B* **1994**, *50*, 17953−17979.
(34) Kresse, G.; Joubert, D. From ultrasoft pseudopotentials to the projector augmented-wave method. *Phys. Rev. B* **1999**, *59*, 1758−1775.
(35) Wippermann, S.; Schmidt, W. G. Entropy Explains Metal-Insulator Transition of the Si(111)-In Nanowire Array. *Phys. Rev. Lett.* **2010**, *105*, No. 126102.

https://dx.doi.org/10.1021/acsomega.0c06019
ACS Omega 2021, 6, 6297−6304